The Meteoritical Society

Meteoritics & Planetary Science 48, Nr 5, 730–743 (2013)
doi: 10.1111/maps.12097

Wüstite in the fusion crust of Almahata Sitta sulfide-metal assemblage MS-166: Evidence for oxygen in metallic melts

Marian HORSTMANN[1*], Munir HUMAYUN[2], Dennis HARRIES[3,4], Falko LANGENHORST[4], Nancy L. CHABOT[5], Addi BISCHOFF[1], and Michael E. ZOLENSKY[6]

[1]Institut für Planetologie, Westfälische Wilhelms-Universität Münster, Wilhelm-Klemm-Str. 10, 48149 Münster, Germany
[2]National High Magnetic Field Laboratory & Department of Earth, Ocean and Atmospheric Science, Florida State University, 1800 E. Paul Dirac Drive, Tallahassee, Florida 32310, USA
[3]Bayerisches Geoinstitut, Universität Bayreuth, Universitätsstraße 30, 95447 Bayreuth, Germany
[4]Institut für Geowissenschaften, Friedrich-Schiller-Universität Jena, Carl-Zeiss-Promenade, 07745 Jena, Germany
[5]Johns Hopkins University Applied Physics Laboratory, 11100 Johns Hopkins Road, Laurel, Maryland 20723, USA
[6]ARES, NASA Johnson Space Center, Houston, Texas 77058, USA
[*]Corresponding author. E-mail: marianhorstmann@uni-muenster.de

(Received 05 September 2012; revision accepted 30 January 2013)

Abstract–Meteorite fusion crusts form during the passage of a meteoroid through the Earth's atmosphere and are highly oxidized intergrowths as documented by the presence of e.g., oxides. The porous and irregular fusion crust surrounding the Almahata Sitta sulfide-metal assemblage MS-166 was found highly enriched in wüstite ($Fe_{1-x}O$). Frictional heating of the outer portions of the assemblage caused partial melting of predominantly the Fe-sulfide and minor amounts of the outer Ni-rich portions of the originally zoned metal in MS-166. Along with melting significant amounts of oxygen were incorporated into the molten fusion crust and mainly FeS was oxidized and desulfurized to form wüstite. Considerable amounts of FeS were lost due to ablation, whereas the cores of the large metal grains appear largely unmelted leaving behind metal grains and surrounding wüstite-rich material (matte). Metal grains along with the surrounding matte typically form an often highly porous framework of globules interconnected with the matte. Although textures and chemical composition suggest that melting of Fe,Ni metal occurred only partially (Ni-rich rims), there is a trace elemental imprint of siderophile element partitioning influenced by oxygen in the metallic melt as indicated by the behavior of W and Ga, the two elements significantly affected by oxygen in a metallic melt. It is remarkable that MS-166 survived the atmospheric passage as troilite inclusions in iron meteorites are preferentially destroyed.

INTRODUCTION

Fusion crusts surrounding meteorites form as a result of melting of the outermost portions of the meteoroid triggered by frictional heating during its passage through the Earth's atmosphere. Fusion crust mineralogy mirrors very oxidizing conditions as documented by e.g., the presence of oxides such as magnetite or wüstite. Wüstite ($Fe_{1-x}O$) is a rare opaque iron oxide in terrestrial rocks, but can be found in meteorite fusion crusts and products of metallurgy. It has a cubic (NaCl) crystal structure and is a member of the periclase group. At low pressures, this mineral is almost exclusively nonstoichiometric due to the presence of Fe^{3+} on the octahedral sites replacing Fe^{2+} and a number of vacancies, depending on temperature and oxygen fugacity (fO_2) (Lindsley 1976, 1991; Wriedt 1991). Wüstite is metastable at room temperature and stable only above ~570 °C at 1 bar, the eutectoid equilibrium temperature of wüstite–α-Fe–magnetite (Lindsley 1976). Its specific stability field (low-fO_2 and high-T) and its preference to react with silicates under all but the most silica-undersaturated environments (e.g., metallic melt systems) account for its rarity in crustal rocks (Lindsley 1991). Wüstite has been described in or closely related to meteorite fusion crusts (e.g., El Goresy and Fechtig 1967; Ramdohr 1967; Genge and Grady

1999; Kim et al. 2009) surrounding various types of meteorites. Ramdohr (1967) gives an overview of meteorite fusion crusts and El Goresy and Fechtig (1967), for example, provide insights into the layered structure of wüstite-bearing fusion crusts found in iron meteorites and mesosiderites. Genge and Grady (1999a) present a comprehensive survey of stony meteorite fusion crusts. In chondritic meteorites, for instance, wüstite appears in the innermost melted crust and typically forms the cores of magnetite grains (Ramdohr 1967; Genge and Grady 1999). Furthermore, wüstite is known as a constituent in I-Type cosmic spherules or meteorite ablation spheres (e.g., Brownlee 1985; Genge and Grady 1999a; Rochette et al. 2008) and as a layer around molten kamacite in clasts from the Pampa del Infierno chondrite (Boctor et al. 1982). In many instances, wüstite is the product of partial oxidation of metal, but still a relatively rare phase. Texturally and morphologically, meteorite fusion crusts can be quite variable. Krinov (1960) gives an overview of fusion crusts ranging from smooth to knobby, ribbed to striated, to net-like or porous in texture.

MS-166 is one single stone that belongs to the hundreds of meteorite fragments collected in the Almahata Sitta strewn field representing the remnants of asteroid 2008 TC_3 that impacted Earth in October 2008 (Jenniskens et al. 2009). Examination of this and about 70 other fragments revealed a large variety of different chondritic and achondritic samples (Bischoff et al. 2010; Horstmann et al. 2010, 2012a). MS-166 is a fusion-crusted individual (3.25 g, $\sim$1.5 $\times$ 1 cm) that consists of a unique sulfide-metal assemblage with minor ureilitic silicate portions enclosed. These portions are similar in composition to other fine-grained Almahata Sitta ureilites (Bischoff et al. 2010). As pointed out by Bischoff et al. (2010) such sulfide-metal assemblages have never before been found in any meteorite. Additionally, the fusion crust of the MS-166 sample was found to be very irregular and vesicular, which is different from most other pieces in the Almahata Sitta collection studied at the Institut für Planetologie, Münster. Initial examination of mm-sized pieces from MS-166 provided to us without contextual information revealed the presence of a wüstite-bearing lithology the context of which was mistaken as an interior fragment (Horstmann et al. 2012b, 2012c). In this study, subsequent examination of the complete MS-166 specimen revealed that the wüstite-bearing lithologies were fragments taken from the fusion crust surrounding the unusual metal-sulfide assemblage. In the MS-166 fusion crust studied here, wüstite is highly abundant in a quench-textured troilite-wüstite metallic liquid.

It is the purpose of this article to report on the morphological and textural as well as the mineralogical and chemical characteristics of the MS-166 fusion crust with particular emphasis on the high abundances of wüstite and its structural and chemical properties. Furthermore, possible effects on siderophile element partitioning in the molten fusion crust under influence of oxygen preserved as wüstite will be evaluated. Oxygen is a potentially important element in metallic melt systems as it can have an effect on elemental partitioning (Chabot and Humayun 2011). Oxygen-bearing metallic melt systems have been reported in other meteorite fusion crusts and I-Type cosmic spherules. Trace element partitioning influenced by oxygen has been evoked to explain elemental fractionation among I-Type cosmic spherules (e.g., Nozaki et al. [1999] and references therein) and elemental fractionations in meteorite fusion crusts (Genge and Grady 1999).

Initial results of our study have been presented in Horstmann et al. (2012b, 2012c).

SAMPLE AND ANALYTICAL METHODS

Optical examinations were performed on the complete original specimen of MS-166 (Figs. 1 and 2) covered by a highly irregular and vesicular fusion crust (cf. Fig. 1). Thin and thick sections were prepared from broken off fusion crust pieces and from a slice taken through the main mass. Details were obtained in reflected light using a Zeiss-Axiophot and a Keyence 3D (Keyence VHX-500F) polarizing microscope.

The fusion crust pieces were subsequently studied by electron microscopy using a JEOL 6610-LV scanning electron microscope at the Interdisciplinary Center for Electron Microscopy (ICEM), Münster. Quantitative mineral analyses for metal, sulfide, and silicates were obtained using a JEOL JXA 8900 Superprobe electron microprobe (EPMA) at the ICEM operated at 15 keV and a probe current of 15 nA. Natural and synthetic standards of well-known compositions were used as standards for wavelength dispersive spectrometry. These were jadeite (Na), sanidine (K), diopside (Ca), kyanite (Al), fayalite (Fe), chromium-oxide (Cr), Ni-oxide (Ni), hypersthene (Si), San Carlos olivine (Mg), rhodonite (Mn), and rutile (Ti) for silicates. For the analyses of sulfide (large masses of FeS in MS-166), the following elements were measured: jadeite (Na), sanidine (K), diopside (Ca), chromium-oxide (Cr), San Carlos olivine (Mg), hypersthene (Si), rhodonite (Mn), chalcopyrite (Cu, S), pentlandite (Ni), pyrite (Fe), sphalerite (Zn), and Co-metal (Co). The same elements were monitored for metal with the following differences regarding standards: metal standards (Astimex) were used for Fe, Ni, and Si; S was taken from pentlandite. The matrix corrections were made according to the CITZAF procedure of Armstrong (1995).

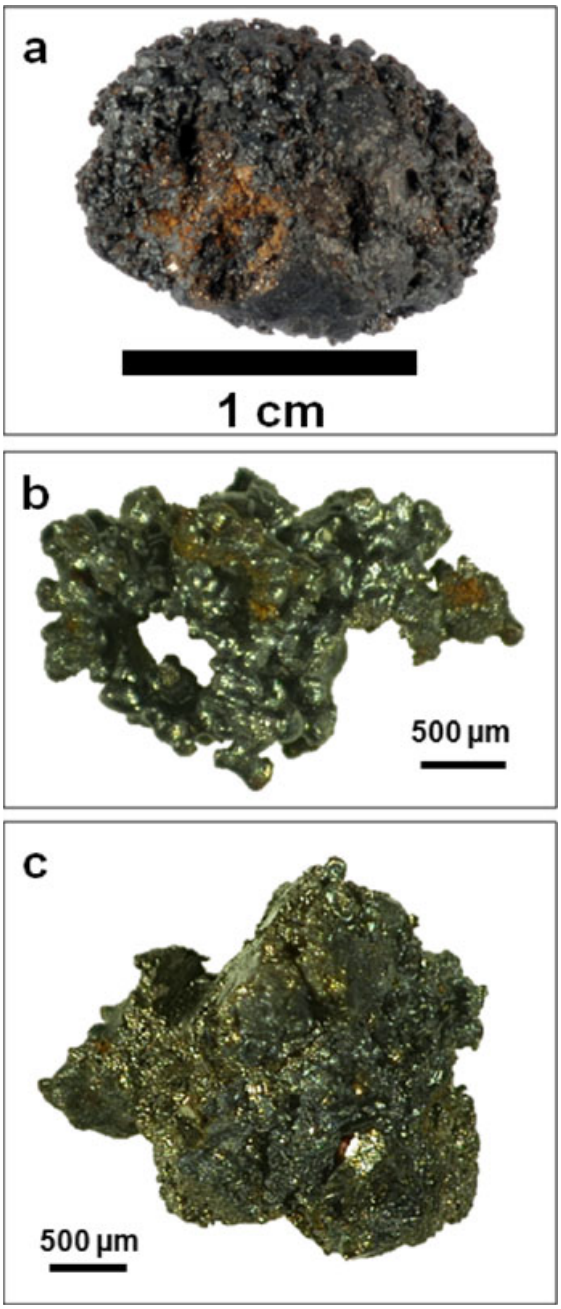

Fig. 1. Overview of the MS-166 specimen and fusion crust material. a) MS-166 bulk sample measuring ~1.5 × 1 cm and weighing 3.25 g. The brownish area (see colored online version) marks the portion from which material was broken off and studied by Bischoff et al. (2010) and Horstmann et al. (2012b). Clearly visible is the very uneven and porous fusion crust. b) Fragment of the fusion crust showing a porous framework of mainly rounded globules (Fe,Ni-metal). These are connected by the wüstite-bearing material. c) A more coherent and compact piece of the fusion crust.

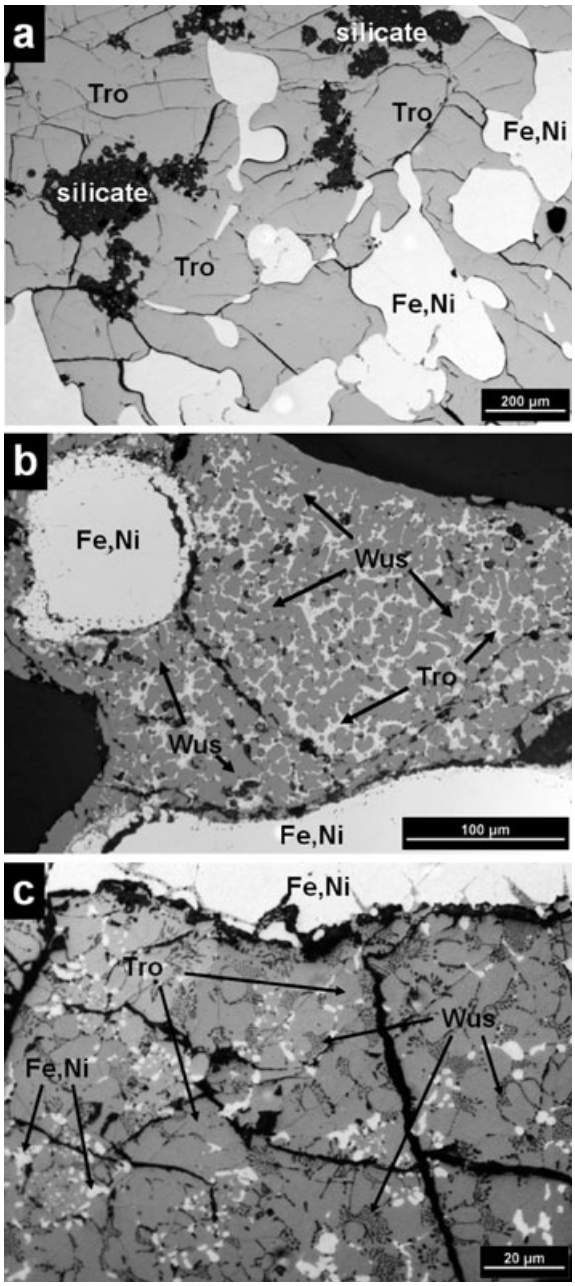

Fig. 2. Different portions of MS-166. a) Section from the FeO-free unaltered main mass. Metal grains (Fe,Ni) and ureilitic material (silicate) appear embedded in masses of troilite (Tro). b) Typical portion of the fusion crust. Metal grains showing corroded outer portions are surrounded by an intergrowth of rounded to elongated grains of wüstite (Wus), interstitial troilite (Tro), and tiny mainly Ni-rich metal grains. c) Transitional low-oxygen zone. Troilite appears as rounded grains with interstitial droplets of Fe-oxide. See text for details. Reflected light images.

Laser ablation-inductively coupled plasma-mass spectrometry measurements were performed at the NHMFL Plasma Analytical Facility, Florida State University, following the procedures described in e.g., Humayun et al. (2007, 2010) and Gaboardi and Humayun (2009). All trace element measurements

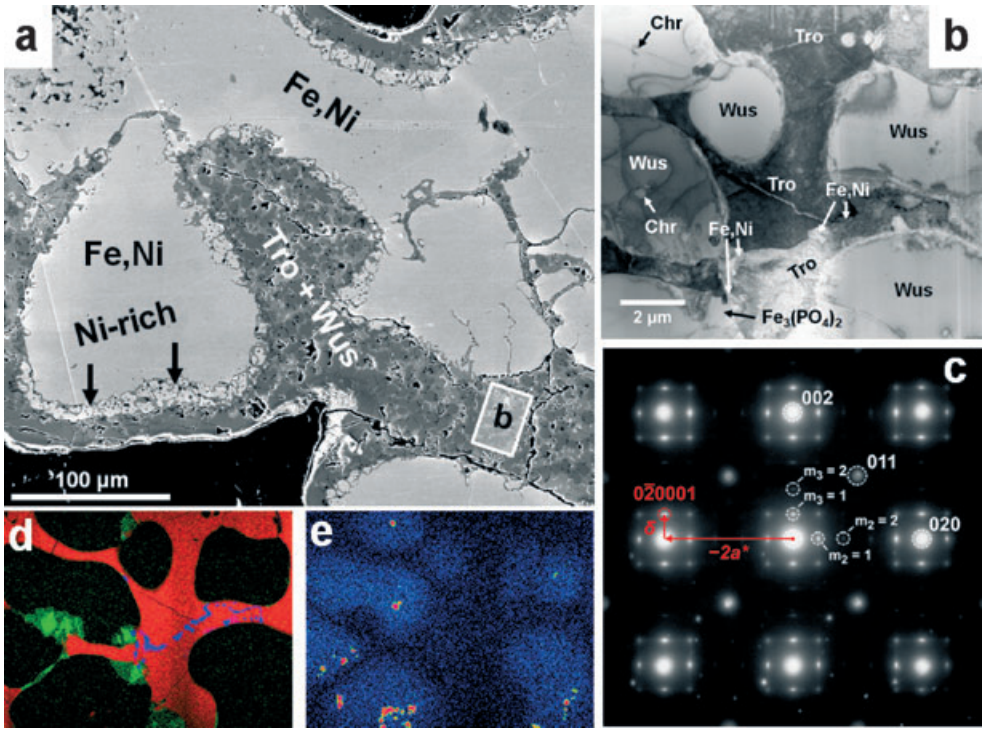

Fig. 3. a) Overview of the MS-166 wüstite-rich fusion crust showing large metal grains surrounded by Ni-rich nuggets embedded in an intergrowth of troilite (Tro) and wüstite (Wus) from which the FIB-section was separated (area indicated by (b)). Secondary electron image. b) TEM-bright field image from the portion separated by FIB technique (area shown in (a)) illustrating the different minerals and the textural context, and revealing the presence of additional chromite (Chr) and an Fe-phosphate ($Fe_3(PO_4)_2$). c) Zone axis [100] SAED pattern of MS-166 wüstite (H658) showing the fundamental NaCl-type reflections (002, 020, etc.), symmetry-forbidden reflections (011, etc.), and superstructure reflections (labeled by order m_i). Indexing of superstructure reflections is shown exemplarily (red). d) TEM-EDX X-ray mapping highlighting the different constituents shown in (b): red = FeS, green = Phosphate, blue = Ni-rich metal. Black areas are wüstite. Horizontal width = 13.5 µm. e) TEM-EDX X-ray mapping of the same area as in (d) illustrating the Cr concentration. Red = high (chromite grains), blue/black = low (wüstite/troilite). Horizontal width = 13.5 µm.

reported here were conducted on a New Wave UP193FX excimer laser ablation system (193 nm) coupled to a ThermoFisher Element XR sector-field ICP-MS. The following trace element measurements were monitored in low resolution mode: ^{29}Si, ^{31}P, ^{34}S, ^{57}Fe, ^{59}Co, ^{60}Ni, ^{63}Cu, ^{69}Ga, ^{74}Ge, ^{75}As, ^{95}Mo, ^{103}Rh, ^{106}Pd, ^{120}Sn, ^{121}Sb, ^{184}W, ^{185}Re, ^{192}Os, ^{193}Ir, ^{195}Pt, and ^{197}Au. Standards used for conversion of intensities into concentrations included the iron meteorites North Chile IIA (Filomena specimen) and Hoba IVB (Wasson et al. 1989; Campbell et al. 2002), NIST SRM 610 silicate glass, NIST SRM 1263a steel, and the USGS basalt glass reference materials BHVO-2G, BCR2-G, and GSE-1G. Standards were measured in line or raster scan mode with the following laser conditions: 50 µm spot size, 10 µm s^{-1} travel speed, 20 Hz repetition rate, and 100% laser energy output. The raster scans were performed with 50 µm spacing.

The samples were ablated in spot mode with spot sizes of 50 µm or 100 µm. The dwell time was set at 2 s for all measurements to avoid sample truncation and contamination of material from the mounting material holding the meteorite sample and from the glass slide below. Measurements showing contamination effects from sample truncation were excluded. Uncertainties for the inferred relative sensitivity factors (RSF) were calculated as two times the standard deviation of three RSFs calculated from three measurements divided by the average RSF of the three single values. The uncertainties on the RSFs for all elements range from ~2 to 20%, but were predominantly below ~10%. Detection limits were calculated from three standard deviations of the measured blank intensities obtained in the same analytical session. The trace element abundances were substituted for the detection limit in cases where the concentration was below it and are indicated in the tables listing the abundances.

A selected portion of the intergrowth between the large metal grains (Fig. 3) was separated by focused ion beam (FIB) technique and subsequently studied by transmission electron microscopy (TEM) at Bayerisches Geoinstitut, University Bayreuth. The FIB cut was

conducted with a FEI Quanta 3D FEG machine using Ga^+ ions. The sample site was covered with a Pt coating to protect it during cutting. The cut was lifted out after thinning to ~1 μm. Final thinning down to ~250 nm was performed on the Cu FIB-TEM grid at 30 kV and 100 pA. Further thinning was applied after the first round of TEM investigations at 50 kV and 80 pA down to a final thickness of ~100 nm. For mineral identification and characterization on a submicron scale, we used a Philips CM20 FEG TEM operated at 200 kV and equipped with a Thermo-Noran EDX and Gatan PEELS spectrometer. Fe L_{32} electron energy loss spectra (EELS) were measured to determine the Fe^{2+}/Fe^{3+} ratio in wüstite (Heidelbach et al. 2003).

RESULTS

Hand Specimen Examination

Almahata Sitta MS-166 is a black ovoid rock (Fig. 1a) weighing 3.25 g that is completely covered by a black, very irregular, and vesicular fusion crust (Figs. 1a and 1b). It measures about 1.5 × 1 cm. Within voids, small grains of terrestrial material in the form of quartz and feldspar grains from the Nubian Desert were encountered. Minor portions of the sample surface are covered by a slight brownish taint indicating minor terrestrial oxidation. These are those parts from which material studied by Bischoff et al. (2010) and Horstmann et al. (2012b) was broken off (Fig. 1a, see colored online version). The fusion crust itself consists of a framework of interconnected slightly rounded to elongated globules (Figs. 1b and 1c) that appear at different packing densities. Some portions are very coherent with less porosity; others are much more porous (cf. Figs. 1b and 1c). Only very minor areas of the fusion crust are rather smooth.

Textures and Mineralogy in Thin Section

First results on the mineralogy and chemistry of the fusion crust assemblage have been reported by Bischoff et al. (2010). Further details are given in Horstmann et al. (2012b).

Wüstite was solely found in the fusion crust of MS-166 (Figs. 1 and 2 and Bischoff et al. 2010; their figs. 4c and 4d). MS-166 was identified as a unique sulfide-metal assemblage (Bischoff et al. 2010) showing a texture of rounded to elongated metal grains embedded in large masses of FeS (0.6–0.8 wt% Ni, up to ~0.2 and ~0.3 wt% Co and Cr, respectively, Fig. 2a). Metal is chemically zoned in Ni (cores: 7–10 wt% Ni, rims: up to ~32 wt% Ni) and siderophile trace elements (Bischoff et al. 2010; Horstmann et al. 2011; and unpublished data). Silicate material, ureilitic in composition, appears as small patches mainly within sulfide (Fig. 2a). The modal proportions of the three components were determined to be ~65 vol% FeS, ~30 vol% Fe,Ni metal, and ~5 vol% silicates. Thin sections of fusion crust material (Figs. 2b and 2c) surrounding this intergrowth reveal large (up to ~700 μm) irregularly zoned metal grains (cores: 7–9 wt% Ni) with Ni-rich portions (up to ~23 wt% Ni) surrounded by small Ni-rich metal nuggets (5–20 μm; up to ~33 wt% Ni) embedded in an intergrowth of troilite, wüstite, and minor tiny, often Ni-rich metal grains (Figs. 2b and 3). This assemblage will be referred to as matte in the following, a term used in metallurgy for impure fused material consisting of metal and sulfide. The interface of the large metal grains and the surrounding small Ni-metal nuggets exhibits irregular cracks that penetrate several micrometers into the host metal (Figs. 2c and 3a). The irregular outer portions of the large metal grains with the Ni-rich nuggets of irregular shape surrounding them suggest that the outer portions of the metal are partly resorbed by the surrounding matte during fusion. Chemically, the cores and Ni-rich portions in both the fusion crust portions and the unaffected MS-166 interior are very similar, although the textural appearance of the Ni-rich rims is distinct. The ureilitic material (olivine: $Fa_{3–14}$, pyroxene: $Fs_{2–13}Wo_{0.5–1.5}$) frequently encountered in the center of the sample was only found in one portion of the fusion crust attached to the assemblage. Wüstite occurs as rounded to elongated crystals intergrown with interstitial FeS and minor Ni-rich metal (Figs. 2b and 3a). The average oxygen content of the assemblage was determined to be ~12 wt% O (range 8–18 wt%). Surrounding the FeO-rich fusion crust an almost continuous layer of wüstite is developed that itself is encircled by a thin Fe-oxide layer giving lower totals than wüstite that is likely magnetite. One portion intermediate to the FeO-free portion and the wüstite-bearing fusion crust of MS-166 shows troilite as slightly rounded grains with an interstitial filling of tiny wüstite droplets and small metal grains (Fig. 2c), texturally bearing similarities to locally restricted dendritic assemblies. The oxygen content is lower in this portion (average ~3 wt%, range 1.5–4.5 wt%). The latter wüstite-bearing textures resemble (quenched) experimental liquids in an O-bearing metallic liquid (Chabot and Humayun 2011). The rounded droplet-like morphologies of wüstite in both portions (cf. Figs. 2b, 2c, and 3a) and FeS (Fig. 2c) in the low-oxygen portion suggest that they were molten and that wüstite was immiscible in the circumjacent S-rich melt.

Mineral Identification and Characterization on a Submicron Scale

To unequivocally prove the presence of wüstite and to characterize the wüstite-sulfide-metal intergrowth

Table 1. Values obtained for the fundamental lattice vector $\boldsymbol{a}^*$ and the superstructure vector $\boldsymbol{\delta}$ for the listed zone axis of MS-166 wüstite.

Pattern	Zone axis	a^* (nm^{-1})	δ (nm^{-1})	δ/a^*
H658	[100][a]	2.274 ± 0.017	0.893 ± 0.009	0.393 ± 0.005
H658	[100][a]	2.315 ± 0.008	0.912 ± 0.004	0.394 ± 0.002
H651	[110]	2.312 ± 0.014	0.907 ± 0.008	0.392 ± 0.004

Confidence intervals of the means are given at the 95% level.

[a]Obtained from the two orthogonal lattice rows. The lattice constants might indicate a slight distortion from the ideal cubic state, but this could also be imposed by the TEM's electron optics or the film. The δ/a^* parameter is not affected by such instrumental effects and deemed accurate, because systematic errors should affect δ and a^* in the same way and cancel out in the ratio.

interstitial to the large metal grains, a portion of the intergrowth was separated applying FIB technique (location indicated in Fig. 3a). The section was subsequently studied by TEM (Fig. 3b).

Wüstite ($Fe_{1-x}O$)

Selected area electron diffraction (SAED) patterns obtained from the rounded Fe-oxide crystals (Fig. 3b) clearly identify them as nonstoichiometric, i.e., Fe-deficient, wüstite. Diffraction patterns of zone axis [100] show the fundamental NaCl-type reflections (e.g., 020, 002) surrounded by superstructure reflections (Fig. 3c). Symmetry-forbidden reflections with mixed odd/even indices (e.g., 011) occur as well, but show no or only weak superstructure reflections. The presence of a superstructure demonstrates the presence of Fe site defect clusters and a Fe/O ratio slightly less than unity. These defect clusters are characterized by vacant octahedral Fe sites and interstitial, tetrahedrally coordinated Fe atoms (e.g., Hazen and Jeanloz 1984).

Depending on Fe-deficit and thermal history, wüstite can occur in several crystallographic versions (e.g., Anderson and Sletnes 1977): The P′ structure of wüstite has an incommensurate superstructure, i.e., the ratio between the fundamental lattice vector $\boldsymbol{a}^*$ and the superstructure vector $\boldsymbol{\delta}$ is not a rational number, because the arrangement of defect clusters is not regular, but aperiodic (Yamamoto 1982). Each superstructure reflection can be indexed by six integers ($h\ k\ l\ m_1\ m_2\ m_3$): $\boldsymbol{g} = h\boldsymbol{a}^* + k\boldsymbol{b}^* + l\boldsymbol{c}^* + m_1\boldsymbol{\delta}_1 + m_2\boldsymbol{\delta}_2 + m_3\boldsymbol{\delta}_3$. In a cubic lattice, $\boldsymbol{\delta}_i$ should be identical and values reported are between $0.366\boldsymbol{a}^*$ and $0.398\boldsymbol{a}^*$ (Koch and Cohen 1969; Yamamoto 1982). The P″ structure of wüstite is more ordered and commensurate (i.e., $\boldsymbol{a}^*$ and $\boldsymbol{\delta}$ are rational with respect to each other) and shows a corresponding $\boldsymbol{\delta}$ of $0.4\boldsymbol{a}^*$ (Anderson and Sletnes 1977).

On the basis of SAED patterns obtained on the [100] and [110] zone axes, we find the superstructure in MS-166 wüstite to be characterized by an average value of $\boldsymbol{\delta} = (0.393 \pm 0.004)\boldsymbol{a}^*$ (95% confidence or $\sim 2\sigma$, Table 1). This value is close to but still resolved from the commensurate $0.4\boldsymbol{a}^*$. This result indicates a P′ superstructure close to the P″ case. The P″ superstructure forms by slow cooling or subeutectoid aging (Anderson et al. [1984] and references therein), indicating that the MS-166 wüstite had sufficient time to evolve toward the P″ structure. However, significant disorder among vacancy clusters might still be present because only weak higher order superstructure reflections ($m_i > 1$) are observed.

Internally, the wüstite crystals are practically free of dislocations, subgrain boundaries, and planar defects. Each globule-shaped wüstite grain (Figs. 2b, 3a, and 3b) is a single crystal and there appear to be no obvious orientation relationships between neighboring grains. EELS spectra of wüstite grains reveal a relatively high Fe^{3+} content of 16–18% (Fig. 4).

Semi-quantitative TEM-EDX shows that wüstite contains small amounts of chromium (up to ~ 0.5 atom%), which appear to decrease toward the rims of the globules (Fig. 3e). Tiny inclusions of chromite are common within wüstite grains (Figs. 3e and 5a).

Troilite (FeS)

The Fe-sulfide portion (Fig. 3b) was identified to be troilite (stoichiometric FeS) based on a [001] zone axis SAED pattern. Troilite and Fe-deficient pyrrhotite ($Fe_{1-x}S$) show distinct patterns in this orientation. Based on coexistence with Fe-rich metal, troilite is the thermodynamically expected phase (Fe saturation). Troilite in the MS-166 fusion crust shows mottled diffraction contrast and appears to be rich in defects, although individual dislocations could not be imaged clearly. It cannot be ruled out that these defects result from sample preparation. Subgrain boundaries and micro cracks are frequent, but individual troilite crystal domains extend quite widely in between the wüstite globules.

Metal

Metal occurs as dendritic filaments in the troilite (Figs. 3b, 3d, and 5b) and is very Ni-rich based on semiquantitative TEM-EDX (approx. $Ni_{60}Fe_{40}$). No diffraction patterns are available due to the small grain size and strong diffuse scattering owing to foil thickness.

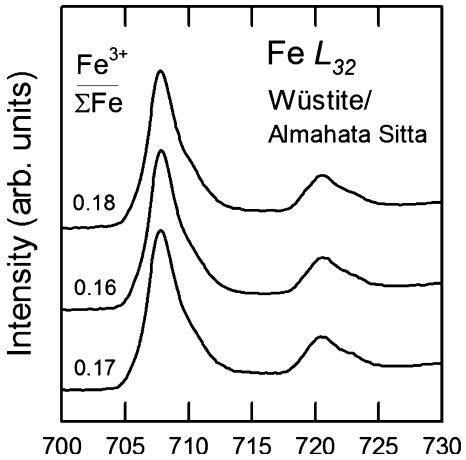

Fig. 4. Electron energy loss spectra (EELS) of MS-166 wüstite grains studied in the separated TEM section. EELS spectra indicate Fe^{3+} contents in MS-166 wüstite of up to 18%. *X*-axis gives the electron energy loss in eV.

Chromite

Tiny chromite grains occur exclusively within wüstite (not in troilite, Figs. 3e and 5a) and have been identified via SAED patterns and TEM-EDX. Mg and Al could not be detected by TEM-EDX. The crystal size ranges between 100 nm and 1 μm.

Fe-Phosphate

TEM-EDX mapping revealed the presence of several angular grains of an Fe-phosphate (Fig. 3d). SAED patterns showed the phosphate to be amorphous. Semi-quantitative TEM-EDX suggests it to have a stoichiometry of either sarcopside or graftonite, both polymorphs of $Fe_3(PO_4)_2$. The empirically derived formula is $(Fe_{2.98},Mn_{0.03},Ca_{0.01})(P_{1.82},Si_{0.12})O_{8.05}$. It is not clear whether the amorphous state is natural or amorphization occurred during sample preparation or TEM-EDX mapping. However, phosphates are commonly quite stable under the electron beam such that rapid quenching is likely the reason for the amorphous state.

Unknown Phase

TEM-EDX showed a mineral phase dominated by Fe and O with little P associated with the Fe-phosphate. SAED patterns yield d-values that closely match wüstite, but intensities appear somewhat atypical for wüstite. In addition, the grains are rather angular and not rounded like typical wüstite in the MS-166 fusion crust. The true phase remains unidentified, but it is either a separate phase or a convolution of wüstite and amorphous Fe-phosphate.

Siderophile Element Abundances

First results on siderophile element systematics in MS-166 have been presented in Horstmann et al. (2011)

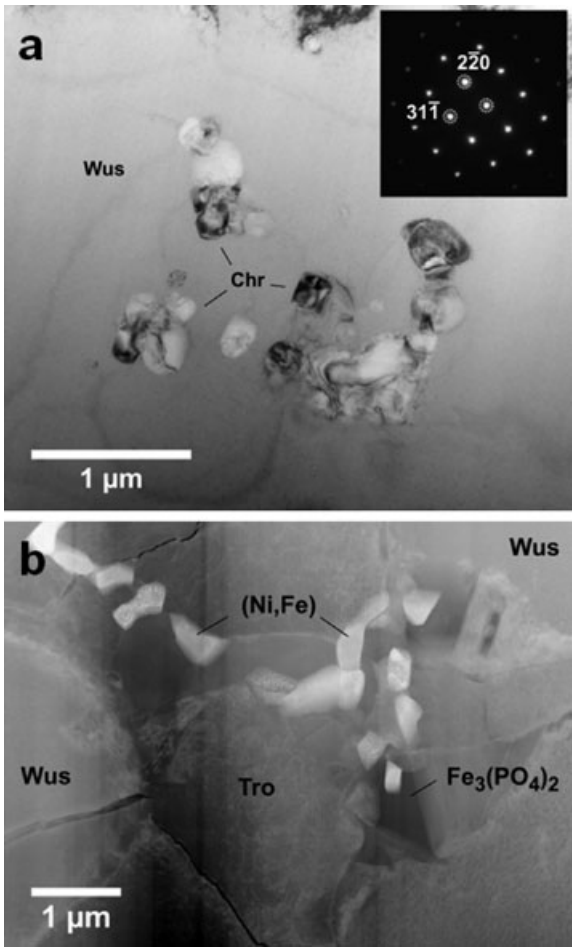

Fig. 5. a) TEM-Bright Field image showing tiny chromite (Chr) grains in MS-166 wüstite (Wus). Inset illustrates the chromite zone axis [114] SAED pattern. b) Scanning TEM-Dark Field image indicating the amorphous Fe-phosphate ($Fe_3(PO_4)_2$) in association with troilite (Tro), wüstite, and Ni-rich metal (Ni,Fe).

and are generally similar to Almahata Sitta sulfide-metal assemblage MS-158. LA-ICP-MS analyses were performed on metal grains (low-Ni cores) in the fusion crust and on the surrounding wüstite-bearing matte. The cores of the metal grains are mainly characterized by convex-upward patterns for the compatible siderophile elements (Fig. 6; e.g., Re, Os, Ir) strongly enriched up to a maximum of 265 × CI for Os (Table 2). However, two metal analyses give rather flat patterns; one even has a negative kink in Os. The surrounding matte exhibits concave-upward patterns for the compatible siderophile elements indicating a strong depletion of Os or Ir by more than two orders of magnitude relative to the metal cores. Antimony and Cu are enriched in the matte relative to the metal grains, whereas Ga and Ge show the opposite trend. In elemental abundances, both Ga and Ge are enriched in the metal relative to the surrounding material (Table 2).

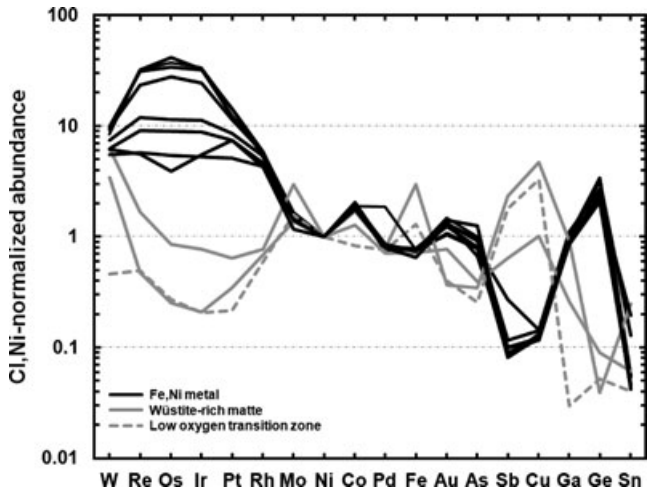

Fig. 6. Siderophile element patterns obtained from low-Ni metal and surrounding FeO-bearing matte in MS-166. Black solid lines are metal analyses, gray solid lines indicate wüstite-rich fusion crust, and dashed line shows siderophile element abundances from the low-oxygen transition zone. Data normalized to CI chondrite and Ni abundances (Anders and Grevesse 1989).

DISCUSSION

Formation of Wüstite

Wüstite has been reported in the inner parts or closely related to several meteorite fusion crusts (e.g., El Goresy and Fechtig 1967; Ramdohr 1967; Genge and Grady 1999; Kim et al. 2009). However, in all these instances, it is neither the only nor the dominant Fe-oxide. Rather magnetite is most prevalent. Thus, the dominance of wüstite needs further consideration. Generally, troilite inclusions within iron meteorites are preferentially destroyed during atmospheric entry as troilite is melted more rapidly than the main mass comprised of metal and/or silicates (Ramdohr 1967). Furthermore, iron meteorites are known to possess broader fusion crusts than stony meteorites because of the high heat conductivity of the metal phase (El Goresy and Fechtig 1967; Ramdohr [1967] and references therein). In this respect, the survival of MS-166 sulfide-metal assemblage is remarkable. However, as will be shown, considerable amounts of predominantly troilite were lost—either ablated or they reacted to FeO.

The main portions of MS-166 are free of any wüstite (Fig. 2a). Consequently, wüstite must be of secondary origin. The presence of wüstite in fusion crusts of iron meteorites is commonly explained by oxidation of metallic Fe along with fusion during atmospheric passage. Oxygen is supplied by the Earth's atmosphere. It is reasonable to assume that material similar to the nonfused, FeO-free portion of MS-166 was the precursor of the wüstite-bearing fusion crust. Comparing the modal abundances of metal and sulfide in the fusion crust (Fig. 2b) and the main rock (neglecting the minor $\sim$5 vol% of silicate in the main mass; Fig. 2a), considerable amounts of FeS (and probably also minor metal) were lost during fusion. FeS was determined to constitute $\sim$65 vol% and metal $\sim$30 vol% of the MS-166 main mass below the fusion crust. However, these proportions have inevitably changed (cf. Fig. 2b) when looking at the fusion crust where the metal grains are the dominant constituent and the wüstite-troilite material is of lower modal abundance ($\sim$75 vol% metal, $\sim$25 vol% FeO-bearing matte). Troilite in the fusion crust makes up only some 10 vol% (Fig. 2b). Metal grains in the fusion crust and those in the unaffected interior of MS-166 are similar in size, shape, and chemical composition (both cores and Ni-rich rims) with the only significant difference that the Ni-rich portions in the fusion crust indicate onset of melt resorption. From this textural and chemical point of view, it is unlikely that all the metal was completely melted as observed in other meteorite fusion crusts (e.g., El Goresy and Fechtig 1967; Genge and Grady 1999). Thus, it seems plausible that wüstite formed in large part from troilite and that considerable amounts of FeS on the order of more than 50% were lost. This ablated material could have given rise to S-rich (and probably even some metal-rich) meteorite ablation spherules (Genge and Grady 1999a).

Formation of wüstite from FeS requires the replacement of S by O as iron in both wüstite and troilite is ferrous. Nevertheless, two possible reactions of importance for MS-166 wüstite formation have to be considered that were given in Asaki et al. (1974) who reported on the oxidation of molten ferrous sulfide:

$$\mathrm{FeS(1)} + \frac{3}{2}\mathrm{O_2} \leftrightarrow \mathrm{FeO(1)} + \mathrm{SO_2} \quad (1)$$

$$\mathrm{Fe(1)} + \frac{1}{2}\mathrm{O_2} \leftrightarrow \mathrm{FeO(1)} \quad (2)$$

As the metal cores appear texturally mainly unmolten, reaction (1) was likely the dominant process taking place in MS-166. However, the outer Ni-rich portions of the metal grains indicate (partial) melting. Thus, reaction (2) might also have contributed to FeO although in minor proportion than FeS. The precipitation of wüstite from an FeS melt undergoing oxidation is furthermore suggested by the eutectic texture of the fusion crust matte. At the surface of meteorite fusion crusts, temperatures of some 1500 °C are likely. Partial melting with generation of an S-rich

Table 2. Siderophile trace element abundances in MS-166 metal and surrounding FeO-bearing matte obtained by LA-ICP-MS. Data reported in ppm. < = values given are measured detection limits.

	Metal								Matte		
	From low-FeO context			From high-FeO context					Low-FeO	High-FeO	
	47-met10	48-met10	49-met11	53-met21	54-met21	55-met21	56-met21	62-met21	31-FeS6	33-FeO	34-FeO
Spot size (μm)	50	50	50	50	50	50	50	50	100	100	50
Si	<1700	<1500	<1500	<1700	<1800	<1600	<1500	2900	<700	700	<4400
P	5300	6900	4900	4200	3700	3800	4500	3800	160	5800	1500
S	2900	<120	<120	610	<140	<130	<120	1800	373000	252000	231000
Fe	903000	915000	918000	921000	919000	921000	919000	911000	598000	682000	753000
Co	6590	6310	6060	6090	6550	6050	6220	6300	1020	3170	1140
Ni	81000	72000	70100	67900	70100	70000	70000	72600	26900	54800	14600
Cu	131	101	96	91	97	94	106	119	1002	637	784
Ga	62	56	57	54	65	61	59	73	1	13	12
Ge	502	455	495	519	706	659	706	582	4	15	<2
As	13	15	12	10	8	10	9	10	1.2	4	<1
Mo	8.0	8.6	8.4	8.9	9.3	8.5	8.7	10	3.6	6.3	3.7
Rh	4.2	3.8	4.5	3.8	4.8	4.6	5.0	5.1	0.19	0.46	<0.1
Pd	3.3	3.1	6.6	2.8	2.8	2.9	2.6	2.8	1.0	2.0	0.59
Sn	<0.6	2.2	<0.5	<0.6	<0.6	1.4	<0.5	0.5	0.2	0.5	<0.6
Sb	0.12	<0.1	<0.1	<0.1	<0.1	<0.1	<0.1	0.25	0.62	0.45	<0.4
W	4.2	3.3	5.0	3.6	5.4	4.3	5.8	5.8	0.10	1.6	0.77
Re	1.5	1.4	7.5	2.0	7.5	2.7	7.3	5.6	0.04	0.09	<0.08
Os	14	17	115	27	129	35	105	89	0.32	0.61	0.55
Ir	19	17	103	26	100	35	98	78	0.24	0.50	0.49
Pt	54	33	88	46	78	54	91	75	0.52	1.7	0.84
Au	1.3	1.3	1.3	1.1	1.2	1.1	0.9	1.0	0.14	0.53	<0.1

metallic melt would start at ~988 °C taking the Fe-FeS system as a basis or would start some 50 °C lower in the Fe-Ni-S system (Villars et al. 1995). 65 vol% FeS corresponds to ~20 wt% S in MS-166. Transferring this to the Fe-S binary would lead to complete melting of MS-166 at around 1300 °C. Taking the amount of Ni into consideration, the temperature might be somewhat lower. Ni-rich metal (taenite) has a lower melting temperature than low-Ni metal (kamacite). Consequently, Ni-rich metal resorption by the metallic melt starts at lower T, which is in textural accordance with what is observed in the MS-166 fusion crust. Taking the Fe-Ni binary system (Schwartzendruber et al. 1991) and the core (7–9 wt% Ni) and rim (~33 wt% Ni) compositions of MS-166 metal grains, the corresponding liquidus temperatures are about 1500–1510 °C and 1460 °C, respectively. This suggests that the temperatures prevailing at the MS-166 surface during fusion were somewhat lower, probably on the order of the above-mentioned ~1300 °C, because the Ni-rich portions show an onset of resorption by the melt and because one is facing a more complex multicomponent system. However, if such elevated temperatures occurred deeper inside the MS-166 rock, fusion would have completely melted the rock. Nevertheless, apparently troilite and only minor metal were effectively molten during atmospheric passage with the majority of FeS material being ablated, some being transformed into FeO, and minor amounts being preserved. Temperatures were either not high enough to cause complete metal melting or the duration of the heating event was too short. The conclusion that the metal cores were largely unmolten (only the outer Ni-rich portions indicate some mobilization) is supported by the siderophile element systematics of the low-Ni cores.

Another argument that predominantly troilite was oxidized to FeO comes from observations made during oxidation experiments of the Gibeon IVA iron meteorite by Visscher and Lodders [2002] and references therein). They found, as other authors before, that Ni in meteoritic metal obviously suppresses wüstite formation, but favors magnetite-spinel formation instead. Nickel is strongly enriched in the outer portions of the metal grains. However, no complete oxidation of FeO into magnetite occurred as observed in the experiments by Asaki et al. (1974). Nevertheless, EELS spectra of wüstite (Fig. 4) in the fusion crust argue for the presence of some Fe^{3+} suggesting at least some oxidation of Fe^{2+} to Fe^{3+}. Darken and Gurry (1945) found a correlation between the Fe^{3+} abundance, temperature, and the composition of the surrounding gas in equilibrium with wüstite. For an Fe^{3+} content on the order of 18% as inferred from the EELS spectra, this leads to a temperature in the range of ~1200 °C (assuming a CO_2/CO of unity). However, this is rather a rough estimate as experimental conditions and procedures differ from what is thought to have taken place during formation of wüstite from FeS in MS-166. The tiny chromite grains found inside wüstite might have formed along with the reaction of troilite to wüstite during fusion as troilite in the main mass was found with minor Cr. However, the abundances were quite low (up to ~0.3 wt% Cr). Similarly, P might have been oxidized and formed the observed Fe-phosphate. The source of P was likely mainly melted Fe,Ni metal from the outer Ni-rich portions from which it was dissolved into and then oxidized in the matte precipitating as the Fe-phosphate upon cooling. LA-ICP-MS analyses on unmelted metal grains gave some 4000 ppm P in the low-Ni cores and can reach even higher values of ~7000 ppm P (Table 2). Trace element analyses on the large FeO-free sulfide masses give P abundances below 100 ppm (unpublished data).

The depth to which temperature was effective in altering the MS-166 meteorite is given by the low-oxygen portions (Fig. 2c). They appear in direct contact with the FeO-free main mass of MS-166 and represent a transition zone in which the effect of fusion and oxidation was less pronounced. Decreasing effects of fO_2 with increasing depth into the meteorite are a typical feature of meteorite fusion crusts (e.g., El Goresy and Fechtig 1967; Genge and Grady 1999). Roundish troilite with tiny droplets of FeO might point to incipient melting or at least recrystallization under elevated temperatures with some oxidation. Partial melting would be supported by Ni-rich nuggets surrounding the metal grains in these areas. The relatively sharp contact of the altered with the unaffected material clearly marks the depth to which heat effectively induced mineralogical changes and is about ~1.5 mm in the portions where the fragile fusion crust was preserved around the cut through the main mass.

The well-ordered state of wüstite close to the P″-type superstructure suggests that cooling took place within a somewhat prolonged time interval. Anderson and Sletnes (1977) report that at 225 °C the P′ structure transforms completely within 30 min to the ordered P″ structure. As our TEM observations indicate a structure close to P″ with some residual disorder, it appears that temperatures in the range between ~200 and 320 °C (below which the ordering phenomena occur) prevailed for some minutes after peak heating. The residual heat might be plausibly explained by the high metal abundance in MS-166 and the correspondingly high heat conductivity, which allowed large volumes of the meteorite to heat up (only partially melting the outer portions) and transfer heat back to the fused, outer portions during dark flight.

The modal abundance of wüstite in the MS-166 fusion crust is remarkable. Although Ramdohr (1967) reported wüstite being prevalent in Fe-rich chondrites, iron meteorites, and mesosiderites, it is commonly found as very small rather rare grains and often intergrown with magnetite. The same author concluded that wüstite can only form and can only be preserved when the supply of FeO increases rapidly, something that was the case with MS-166 via oxidation of large masses of predominantly FeS leaving behind a highly porous framework of metal grains interconnected with Fe-S-O matte.

Partitioning of Siderophile Elements

The unaltered, i.e., nonfused portions of MS-166 (Fig. 2a) were proposed to have formed from a fractionally crystallizing S-rich metallic melt (Horstmann et al. 2011) related to ureilite petrogenesis (Horstmann et al. 2012b). Although the analyzed metal grains are from the fusion crust, they all fall onto the same trend observed for MS-158 metal (Horstmann et al. 2011). Metal from both samples spans nearly three orders of magnitude variation in Ir abundance similar to IIIAB iron meteorites. A negative correlation between Ir and Au is suggestive of a fractional crystallization origin of the metal (Horstmann et al. 2011) with the surrounding troilite-dominated material representing the remaining S-rich liquid. The preserved Ni- and trace element-zoning argues for fast cooling of the material. However, it should be noted that recent, more detailed examinations of MS-166 metal indicate a more complex formation history than only simple fractional crystallization, but this will be the issue of an upcoming article.

Chabot and Humayun (2011) reported on experimental investigations that had the goal of deciphering the influence of oxygen on siderophile trace elemental partitioning in metallic liquids. Oxygen is of considerable importance in planetary differentiation as it is a potential light element in metallic melts probably even in the Earth's core (e.g., Hillgren et al. 2000). Chabot and Humayun (2011) found that elements with affinities to form stable oxides like W and Ga preferentially partition into the oxygen-bearing liquid rather than into the crystallizing metal. This behavior is different from S-rich metallic liquids in which the compatibility in metal of both elements increases with increasing S-content of the melt (e.g., Chabot and Jones 2003; Chabot et al. 2003, 2009). The presence of abundant oxygen preserved as wüstite allows insights into the influence of oxygen on partitioning in a natural sample. Horstmann et al. (2012b) first reported on the presence of wüstite in Almahata Sitta, but reinspection of the entire MS-166 specimen (Horstmann et al. 2012c) revealed that the fragments studied by Horstmann et al. (2012b) sampled mainly fusion crust material, and were thus unrepresentative of the main mass. Therefore, the previous conclusions drawn with respect to ureilite petrogenesis were incorrect. Nevertheless, trace element compositions of metal and surrounding matte could indicate some influence of oxygen on siderophile trace element partitioning. Previously, the effect of oxidation on some elemental abundances has been reported in I-Type cosmic spherules and meteorite fusion crusts (Nozaki et al. [1999] and references therein; Genge and Grady 1999). Here, the first LA-ICP-MS analyses of siderophile trace element partitioning influenced by oxygen in a metallic melt will be presented.

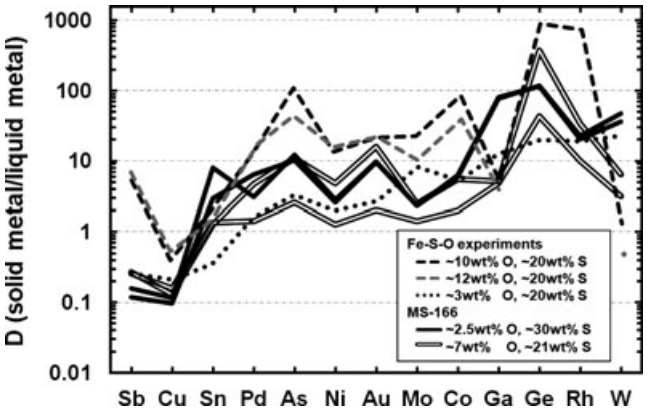

Fig. 7. Comparison of partition coefficients from the Chabot and Humayun (2011) Fe-S-O experiments (black and gray dashed lines correspond to ~10 and ~12 wt% O, respectively, each with ~20 wt% S; dotted line corresponds to ~3 wt% O, ~20 wt% S) and data obtained from MS-166 (black solid lines correspond to ~2.5 wt% O, 30 wt% S, open lines indicate ~7 wt% O, 21 wt% S). See text for details.

Calculated (apparent) distribution coefficients (*D* values) from analyses on metal and matte (Fig. 7) are generally comparable to the experimental results of Chabot and Humayun (2011). It has to be pointed out here that the largely unmelted metal cores were measured and used for calculation of the *D* values, which were likely not in equilibrium with the surrounding matte. This is allowed for by adding "apparent" to the *D* values. The best indicator for the influence of oxygen on elemental partitioning in metallic melts is, as already mentioned, the behavior of W and Ga (Chabot and Humayun 2011), which show decreasing concentrations in the solid metal when oxygen is present in the liquid. As shown in Fig. 7, measurements of the O-rich portion of MS-166, which has ~7 wt% O, show a lower *D* value for W than the O-poor (~2.5 wt% O) MS-166 measurement. This difference is consistent with the elemental partitioning signature expected due to O in a metallic melt. The presence of O in the metallic melt would also impart a

distinctive signature on Ga, and the D(Ga) value for the O-rich measurements of MS-166 is lower than the O-poor ones, consistent with the behavior due to the presence of O in a metallic melt.

Both the S and O contents of a metallic melt will influence the partitioning behavior, and the experimental results presented in Fig. 7 have slightly different S and O contents than measured in the MS-166 analyses. The solid metal-liquid metal partitioning behavior in the Fe-(Ni)-S system has been parameterized (Chabot and Jones 2003) such that one can apply it to the specific S contents measured in the MS-166 analyses. Using the inferred bulk chemical abundances of S for the high-O and low-O portions ($\sim$21 wt% S and $\sim$30 wt% S, respectively) surrounding the metal grains analyzed, the apparent partition coefficients between solid metal and liquid metal for the given compositions in the Fe-S system were calculated (Fig. 8). As mentioned above, the best indicator for the influence of oxygen on elemental partitioning in metallic melts is the behavior of W and Ga (Chabot and Humayun 2011). Figure 8 shows that Ga and W, which are expected to show deviating behavior from the modeled *D* values in the pure Fe-S system corresponding to the shaded area in Fig. 8, do not exhibit clear anomalies. For the low-oxygen portion, it can be concluded that the partitioning is consistent with partitioning in the pure Fe-S system without any obvious indication for influence of oxygen. In the case of the oxygen-rich portions, however, one can see a deviating behavior for both W and Ga relative to Ge and Rh. Both elements show lower apparent D values by about an order of magnitude than in the low-oxygen portion (Fig. 8a). This is also clearly depicted in Fig. 8b, in which the ratio of the apparent *D* values for the high-O and low-O portion is shown. Gallium in the wüstite-rich portion shows a lower *D* value than in the low-oxygen domain, but apparent *D* values for Ga and Ge are much higher than expected from the modeled values using the estimated S abundances for the respectively analyzed portions of MS-166 fusion crust and plot above the shaded area in Fig. 8a, while the Ga value for the high-O portion ends up in the shaded area. Consequently, there is trace elemental evidence for the influence of oxygen on elemental partitioning in the MS-166 fusion crust, although conditions in the fusion crust were certainly nonequilibrium. However, the observed textures in the large metal grains (Fig. 3a) are seemingly not in accordance with complete melting of the fusion crust metal, but rather imply partial dissolution of the Ni-rich rim metal leaving the low-Ni cores largely unaffected, with obvious implications for apparent partition coefficients. As noted earlier, the original texture of the fusion crust material was likely

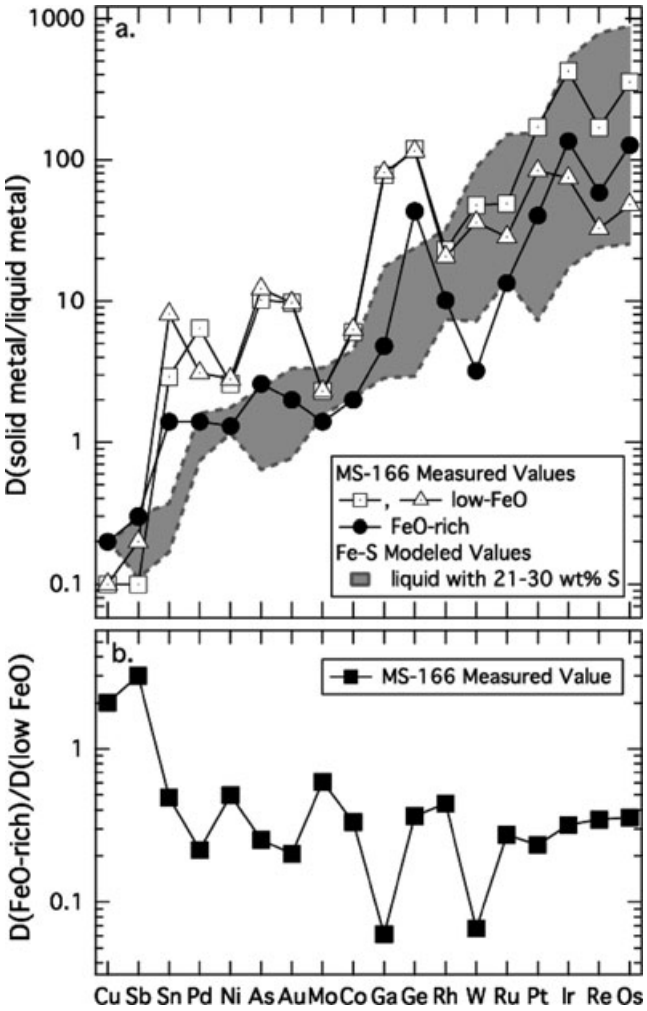

Fig. 8. a) Compilation of modeled and measured (or apparent) $D_{\text{solid metal/liquid metal}}$ values for the FeO-rich and low-FeO portions of MS-166. The D values were modeled for partitioning in the Fe-S system with liquid S-contents that ranged from 21 to 30 wt%, as measured in the matte of MS-166 (shaded area). b) Ratio of apparent D values for the FeO-rich and low-FeO portion illustrating the deviant behavior of W and Ga.

similar to the unaltered main mass of MS-166. Thus, the Ni-rich nuggets surrounding the metal cores might indicate early stages of metal resorption by the S,O-rich melt. LA-ICP-MS measurements of the tiny Ni-rich nuggets surrounding the low-Ni cores were precluded by the small grain size. Thus, no conclusion based on data from these small nuggets can be drawn as to whether the outer metal portions experienced elemental equilibrium partitioning in an oxygen-bearing liquid. Nevertheless, the apparent D values (Fig. 8) indicate that some elemental redistribution took place. Minor amounts (compared with the low-Ni cores) of W and Ga were present in the outer portions of the metal grains that were (partially) resorbed by the Fe-S-O

liquid during fusion crust formation, and thus W and Ga could have preferentially partitioned into the matte upon solidification accounting for the deviant behavior of both W and Ga (Fig. 8). Such a scenario would not require complete melting of the metal grains. In contrast with Fe-sulfide, it appears that the metal cores originally present in the outer portions of MS-166 largely survived the fusion process.

CONCLUSIONS

Large portions of the MS-166 Almahata Sitta sulfide-metal assemblage fusion crust form a highly porous framework of rounded metal globules interconnected with a wüstite-troilite-bearing matte. It is remarkable that MS-166 survived atmospheric entry as troilite inclusions in iron meteorites are preferentially destroyed during atmospheric passage. Wüstite in the fusion crust formed mainly via oxidation and desulfurization of a S-rich metallic liquid. Large portions of the troilite component observed in the main mass of MS-166 were lost during ablation. Textural evidence suggests that the metal grains (cores) were never completely molten, but indicate only minor resorption of the Ni-rich rim portions of the originally zoned metal grains. This is different from other meteorite fusion crusts (e.g., El Goresy and Fechtig 1967; Genge and Grady 1999) in which metal was largely melted. Considerable amounts of oxygen were incorporated into the molten MS-166 fusion crust. Trace siderophile element partitioning behavior of W and Ga (the two elements significantly affected by oxygen in a metallic melt) in the wüstite-rich portions of the MS-166 fusion crust bears evidence of siderophile element partitioning in an oxygen-bearing metallic melt. Thus, it appears that siderophile element redistribution took place only between the molten outer rim and the matte. Fusion temperatures probably prevailed for too short timescales to allow complete melting of the material and subsequent rapid quenching of the molten portions would have also precluded complete equilibration. The better contextual evidence now available by inspection of the main mass of MS-166 reveals that the Fe-S-O liquid played no role in ureilite petrogenesis, contrary to previous suggestions (Horstmann et al. 2012b). Notwithstanding, MS-166 is a natural meteorite sample that bears evidence for siderophile element partitioning influenced by oxygen in a metallic melt.

Acknowledgments—Ulla Heitmann (Münster) is acknowledged for sample preparation. M. J. Genge, an anonymous reviewer, and associate editor E. R. D. Scott provided constructive reviews and very helpful comments that significantly improved the manuscript. This work was partly supported by the German Research Foundation (DFG) within the priority program "The First 10 Million Years of the Solar System—A Planetary Materials Approach" (SPP 1385) and by the NASA Cosmochemistry Program through grants NNX10AI37G (M. Humayun) and NNX12AH88G (N. L. Chabot).

Editorial Handling—Dr. Edward Scott

REFERENCES

Anders E. and Grevesse N. 1989. Abundances of the elements: Meteoritic and solar. *Geochimica et Cosmochimica Acta* 53:197–214.

Anderson B. and Sletnes J. O. 1977. Decomposition and ordering in $Fe_{1-x}O$. *Acta Crystallographica* 33:268–276.

Anderson A. B., Grimes R. W., and Heuer A. H. 1984. Defect clusters in wüstite, $Fe_{1-x}O$. *Journal of Solid State Chemistry* 55:353–361.

Armstrong J. T. 1995. CITZAF: A package of correction programs for the quantitative electron microbeam X-ray analysis of thick polished materials, thin films, and particles. *Microbeam Analysis* 4:177–200.

Asaki Z., Ajersch F., and Toguri J. M. 1974. Oxidation of molten ferrous sulphide. *Metallurgical Transactions* 5:1753–1759.

Bischoff A., Horstmann M., Pack A., Laubenstein M., and Haberer S. 2010. Asteroid 2008 TC_3—Almahata Sitta: A spectacular breccia containing many different ureilitic and chondritic lithologies. *Meteoritics & Planetary Science* 45:1638–1656.

Boctor N. Z., Bell P. M., Mao H. K., and Kullerud G. 1982. Petrology and shock metamorphism of Pampa del Infierno chondrite. *Geochimica et Cosmochimica Acta* 46:1903–1911.

Brownlee D. 1985. Cosmic dust—Collection and research. *Annual Reviews of Earth and Planetary Sciences* 13:147–173.

Campbell A. J., Humayun M., and Weisberg M. K. 2002. Siderophile element constraints on the formation of metal in the metal-rich chondrites Bencubbin, Weatherford, and Gujba. *Geochimica et Cosmochimica Acta* 66:647–660.

Chabot N. L. and Humayun M. 2011. Exploring the influence of oxygen on partitioning in the Fe-S-O system (abstract #1590). 42nd Lunar and Planetary Science Conference. CD-ROM.

Chabot N. L. and Jones J. H. 2003. The parameterization of solid metal-liquid metal partitioning of siderophile elements. *Meteoritics & Planetary Science* 38:1425–1436.

Chabot N. L., Campbell A. J., Jones J. H., Humayun M., and Agee C. B. 2003. An experimental test of Henry's Law in solid metal-liquid metal systems with implications for iron meteorites. *Meteoritics & Planetary Science* 38:181–196.

Chabot N. L., Saslow S. A., McDonough W. F., and Jones J. H. 2009. An investigation of the behavior of Cu and Cr during iron meteorite crystallization. *Meteoritics & Planetary Science* 44:505–519.

Darken L. S. and Gurry R. W. 1945. The system iron-oxygen. I. The wüstite field and related equilibria. *Journal of the American Chemical Society* 67:1398–1412.

El Goresy A. and Fechtig H. 1967. Fusion crust of iron meteorites and mesosiderites and production of cosmic spherules. *Smithsonian Contributions to Astrophysics* 11:391–397.

Gaboardi M. and Humayun M. 2009. Elemental fractionation during LA-ICP-MS analysis of silicate glasses:

Implications for matrix-independent standardization. *Journal of Analytical Atomic Spectrometry* 24:1188–1197.

Genge M. J. and Grady M. M. 1999a. The fusion crusts of stony meteorites: Implications for the atmospheric reprocessing of extraterrestrial materials. *Meteoritics & Planetary Science* 34:341–356.

Genge M. J. and Grady M. M. 1999b. Unequilibrated assemblages of sulphide, metal and oxide in the fusion crusts of the enstatite chondrite meteorites. *Mineralogical Magazine* 63:473–488.

Hazen R. M. and Jeanloz R. 1984. Wüstite (Fe_{1-x} O): A review of its defect structure and physical properties. *Reviews of Geophysics* 22:37–46.

Heidelbach F., Stretton I., Langenhorst F., and Mackwell S. 2003. Fabric evolution during high shear strain deformation of magnesiowüstite ($Mg_{0.8}Fe_{0.2}$)O. *Journal of Geophysical Research* 108:2154, doi:10.1029/2001JB001632

Hillgren V. J., Gessmann C. K., and Li J. 2000. An experimental perspective on the light element in the Earth's core. In *Origin of the Earth and Moon*, edited by Canup R. M. and Rigther K. Tucson, Arizona: The University of Arizona Press. pp. 245–263.

Horstmann M., Bischoff A., Pack A., and Laubenstein M. 2010. Almahata Sitta—fragment MS-CH: Characterization of a new chondrite type. *Meteoritics & Planetary Science* 45:1657–1667.

Horstmann M., Humayun M., and Bischoff A. 2011. Siderophile element patterns of sulfide-metal assemblages from the Almahata Sitta polymict breccia. *Meteoritics & Planetary Science* 46:A101.

Horstmann M., Bischoff A., Pack A., Albrecht N., Weyrauch M., Hain H., Roggon L., and Schneider K. 2012a. Mineralogy and oxygen isotope compositions of new samples from the Almahata Sitta strewn field (abstract #5052). *Meteoritics & Planetary Science* 47:A193.

Horstmann M., Humayun M., Harries D., Langenhorst F., Chabot N. L., and Bischoff A. 2012b. Wüstite in the Almahata Sitta polymict ureilite: Implications for oxygen during asteroidal differentiation (abstract #1876). 43rd Lunar and Planetary Science Conference. CD-ROM.

Horstmann M., Humayun M., Harries D., Langenhorst F., Chabot N. L., Bischoff A., and Zolensky M. E. 2012c. Wüstite in the fusion crust of the MS-166 Almahata Sitta metal-sulfide assemblage (abstract #5324). *Meteoritics & Planetary Science* 47:A194.

Humayun M., Simon S. B., and Grossman L. 2007. Tungsten and hafnium distribution in calcium-aluminum inclusions (CAIs) from Allende and Efremovka. *Geochimica et Cosmochimica Acta* 71:4609–4627.

Humayun M., Davis F. A., and Hirschmann M. M. 2010. Major element analysis of natural silicates by laser ablation ICP-MS. *Journal of Analytical Atomic Spectrometry* 25:998–1005.

Jenniskens P., Shaddad M. H., Numan D., Elsir S., Kudoda A. M., Zolensky M. E., Le L., Robinson G. A., Friedrich J. M., Rumble D., Steele A., Chesley S. R., Fitzsimmons A., Duddy S., Hsieh H. H., Ramsay G., Brown P. G., Edwards W. N., Tagliaferri E., Boslough M. B., Spalding R. E., Dantowitz R., Kozubal M., Pravec P., Borovicka J., Charvat Z., Vaubaillon J., Kuiper J., Albers J., Bishop J. L., Mancinelli R. L., Sandford S. A., Milam S. N., Nuevo M., and Worden S. P. 2009. The impact and recovery of asteroid 2008 TC_3. *Nature* 458:485–488.

Kim H. Y., Choi B.-G., and Rubin A. E. 2009. Wüstite in the DOM 03238 magnetite-rich CO3.1 chondrite: Formation during atmospheric passage (abstract). *Meteoritics & Planetary Science* 44:A109.

Koch F. and Cohen J. B. 1969. The defect structure of $Fe_{1-x}O$. *Acta Crystallographica* 25:275–287.

Krinov E. L. 1960. Principles of meteorites. In *International series of monographs on earth sciences*, edited by Ingerson E., vol 7. New York: Pergamon Press. 535 p.

Lindsley D. H. 1976. The crystal chemistry and structure of oxide minerals as exemplified by the Fe-Ti oxides. In *Oxide minerals*, edited by Rumble D. III, Reviews in Mineralogy, vol. 3. Washington, D.C.: Mineralogical Society of America. pp. 1–60.

Lindsley D. H. 1991. Chapter 3. Experimental studies of oxide minerals. In *Oxide minerals*, edited by Lindsley D. H. Reviews in Mineralogy, vol. 25. Washington, D.C.: Mineralogical Society of America. pp. 69–106.

Nozaki W., Nakamura T., Iida A., Matsuoka K., and Takaoka N. 1999. Trace element concentrations in iron type cosmic spherules determined by the SR-XRF method. *Antarctic Meteorite Research* 12:199–212.

Ramdohr P. 1967. Die Schmelzkruste der Meteoriten. *Earth and Planetary Science Letters* 2:197–209.

Rochette P., Folco L., Suavet C., van Ginneken M., Gattacceca J., Perchiazzi N., Braucher R., and Harvey R. P. 2008. Micrometeorites from the Transantarctic Mountains. *Proceedings of the National Academy of Sciences* 105:18206–18211.

Schwartzendruber L. J., Itkin V. P., and Alcock C. B. 1991. The Fe-Ni (iron-nickel) system. *Journal of Phase Equilibria* 12:288–312.

Villars P., Prince A. and Okamoto H. 1995. *Handbook of ternary alloy phase diagrams: Co-Fe-Ni-Cu-Mg-Sb*. Materials Park, Ohio: ASM International. pp. 10587–10627.

Visscher C. W. and Lodders K. 2002. Oxidation of the Gibeon IVA iron meteorite. *Meteoritics & Planetary Science* 37:A144.

Wasson J. T., Ouyang X., Wang J., and Jerde E. 1989. Chemical classification of iron meteorites: XI. Multi-element studies of 38 new irons and the high abundance of ungrouped irons from Antarctica. *Geochimica et Cosmochimica Acta* 53:735–744.

Wriedt H. A. 1991. The Fe-O (iron-oxygen) system. *Journal of Phase Equilibria and Diffusion* 12:170–200.

Yamamoto A. 1982. Modulated structure of wüstite ($Fe_{1-x}O$) (three-dimensional modulation). *Acta Crystallographica* 38:1451–1456.